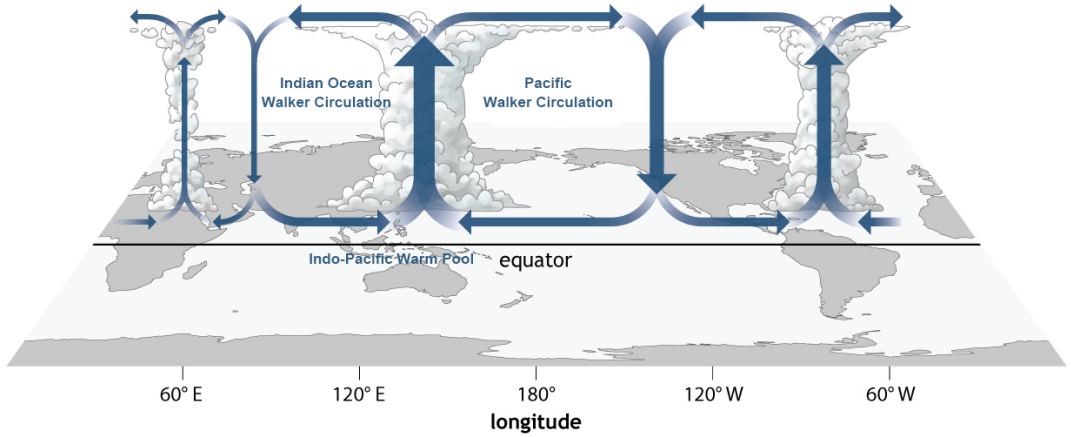
Variations of the Indian Ocean Walker circulation since the Last Glacial Maximum revealed by reconstructed and simulated zonal wind intensity

Xinquan Zhou[1*], Stéphanie Duchamp-Alphonse[1], Masa Kageyama[2], Franck Bassinot[2], Xiaoxu Shi[3], Luc Beaufort[4], Gerrit Lohmann[3]

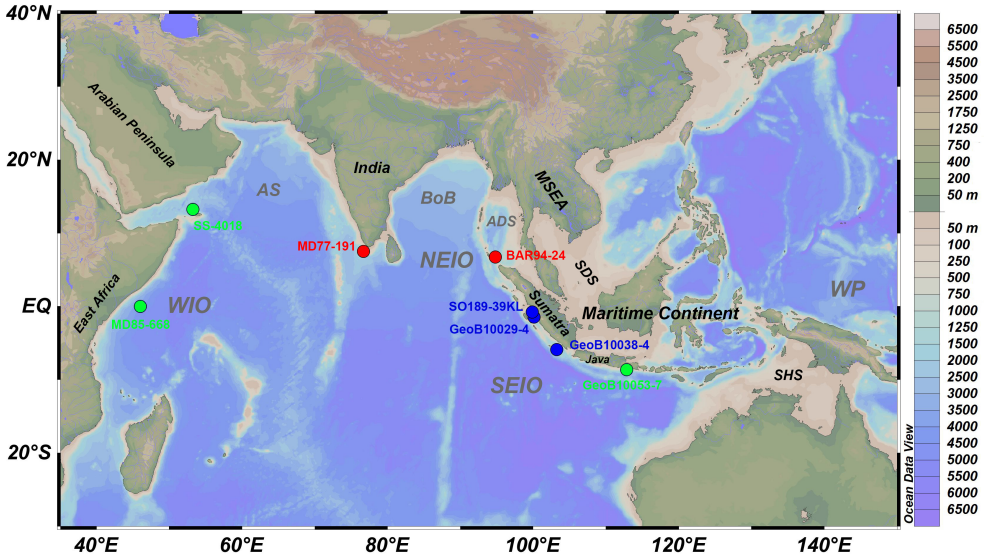
[1]Université Paris-Saclay, GEOPS, CNRS, Orsay, France
[2]LSCE, CEA/CNRS, Gif-sur-Yvette, France
[3]AWI Center for Polar and Marine Research, Bremerhaven, Germany
[4]CEREGE, CNRS/IRD/Aix-Marseille Université, Aix-en-Provence, France

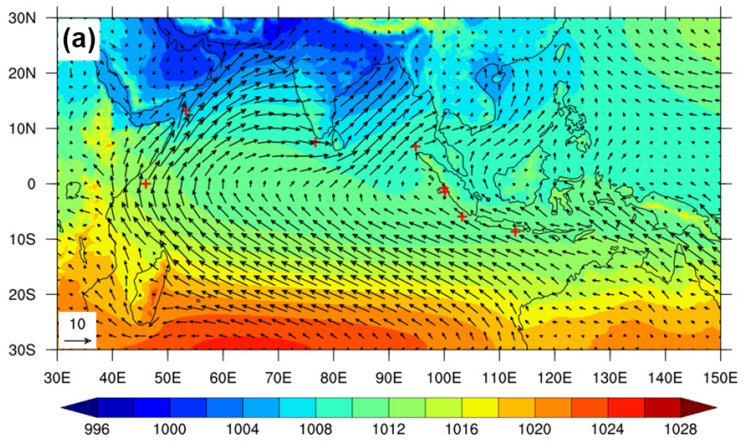
EGU General Assembly 2021

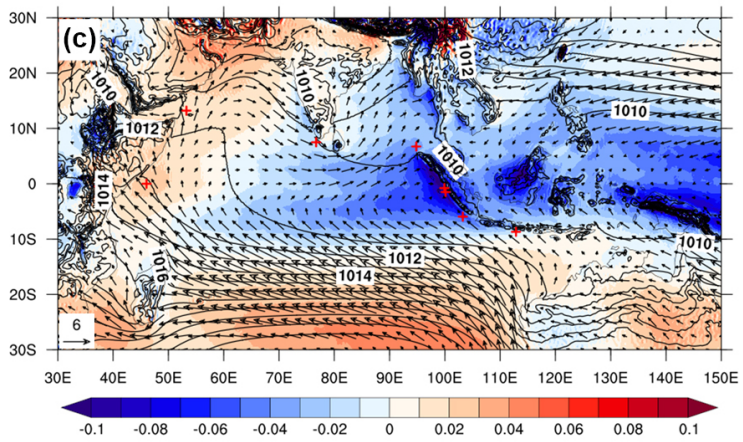
Atmospheric context

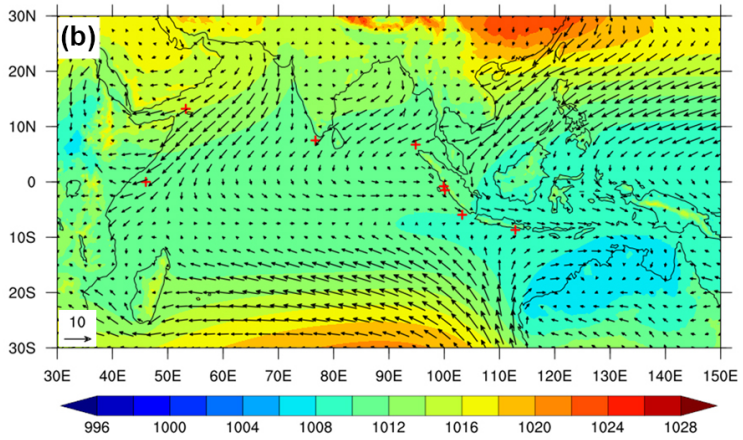


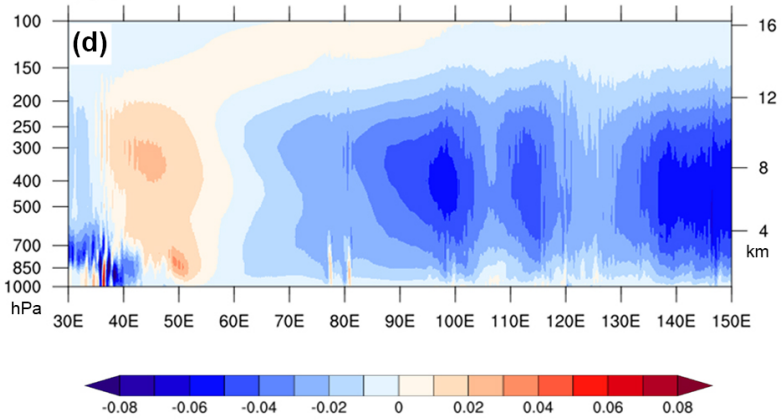
Using marine sediment cores to reconstruct Walker circulation in the past











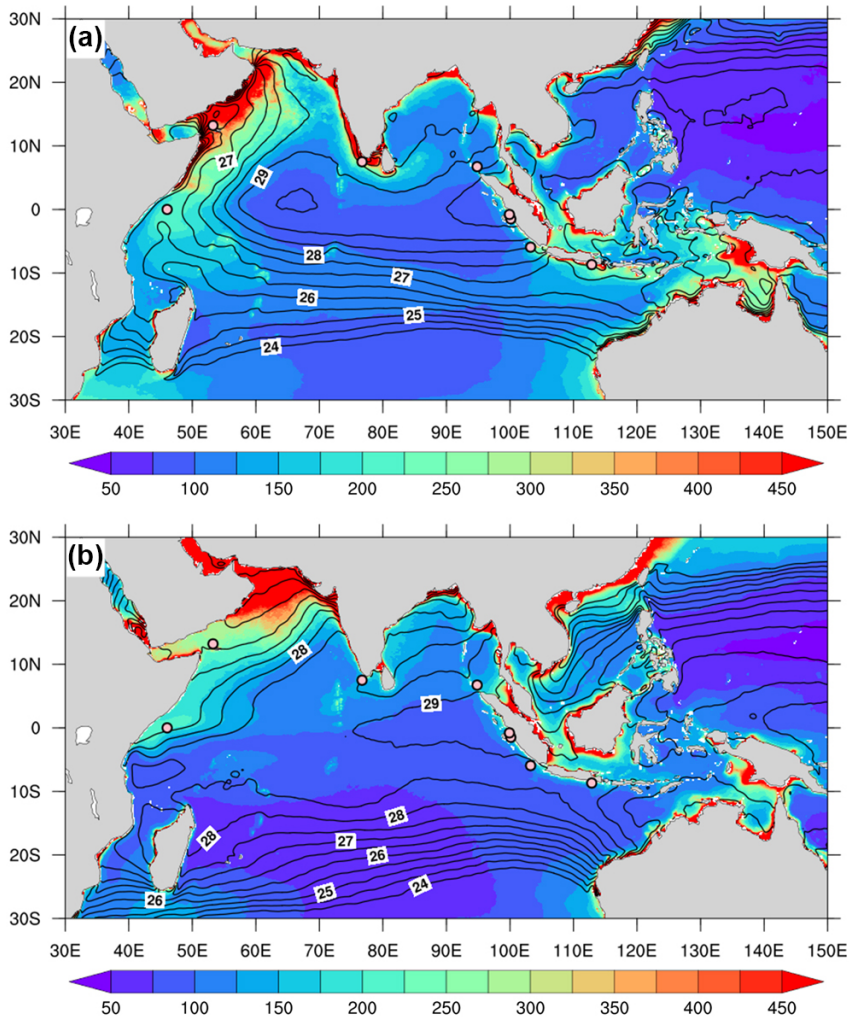
Indian Ocean Walker circulation

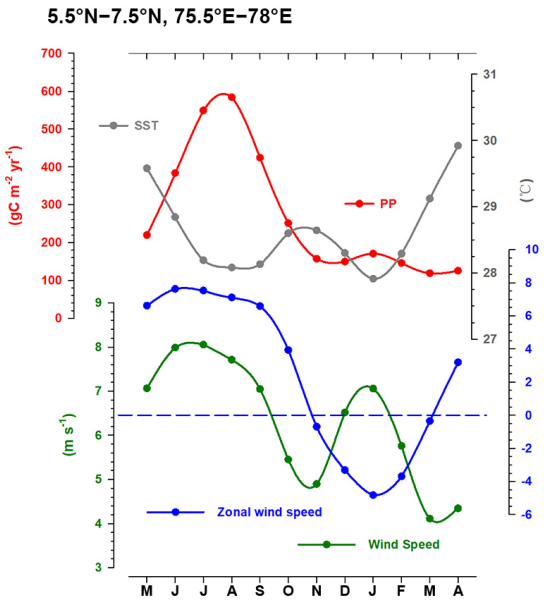
Updraught over the Indo-Pacific Warm Pool
Downdraught over the western Indian Ocean

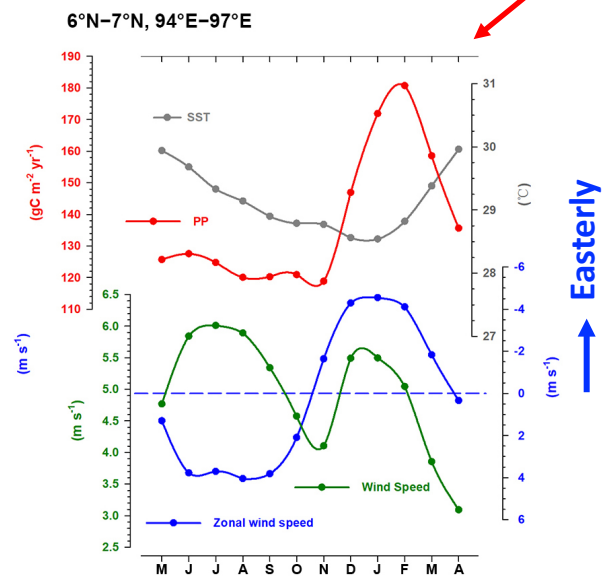
Its seasonal variations are controlled by Indian Monsoon

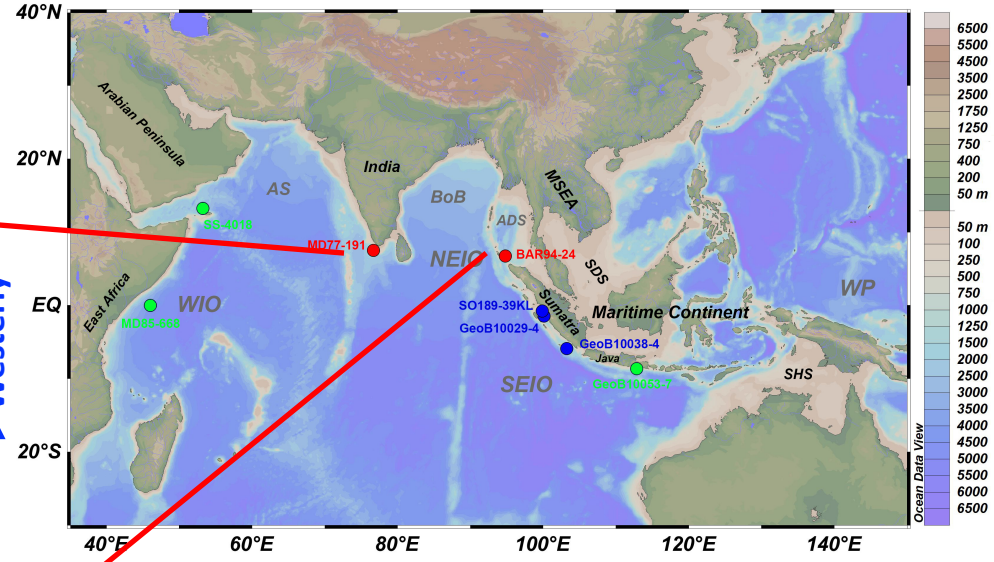
(a) Summer (MJJAS) and **(b)** winter (NDJFM) sea level pressure (color, hPa) and surface wind (vectors, m/s). **(c)** and **(d)** Vertical velocity at 500 hPa (color, Pa/s), surface wind (vectors, m/s), sea level pressure (contours, hPa). Data: ERA5 (1979-2019)

Oceanic settings









Westerly

Easterly

Core MD77-171
Southern tip of Indian,
Westerly-driven upwelling

Core BAR94-24
Northwestern tip of Sumatra,
Easterly-driven upwelling

Primary productivity ⟷ **Paleo-productivity**

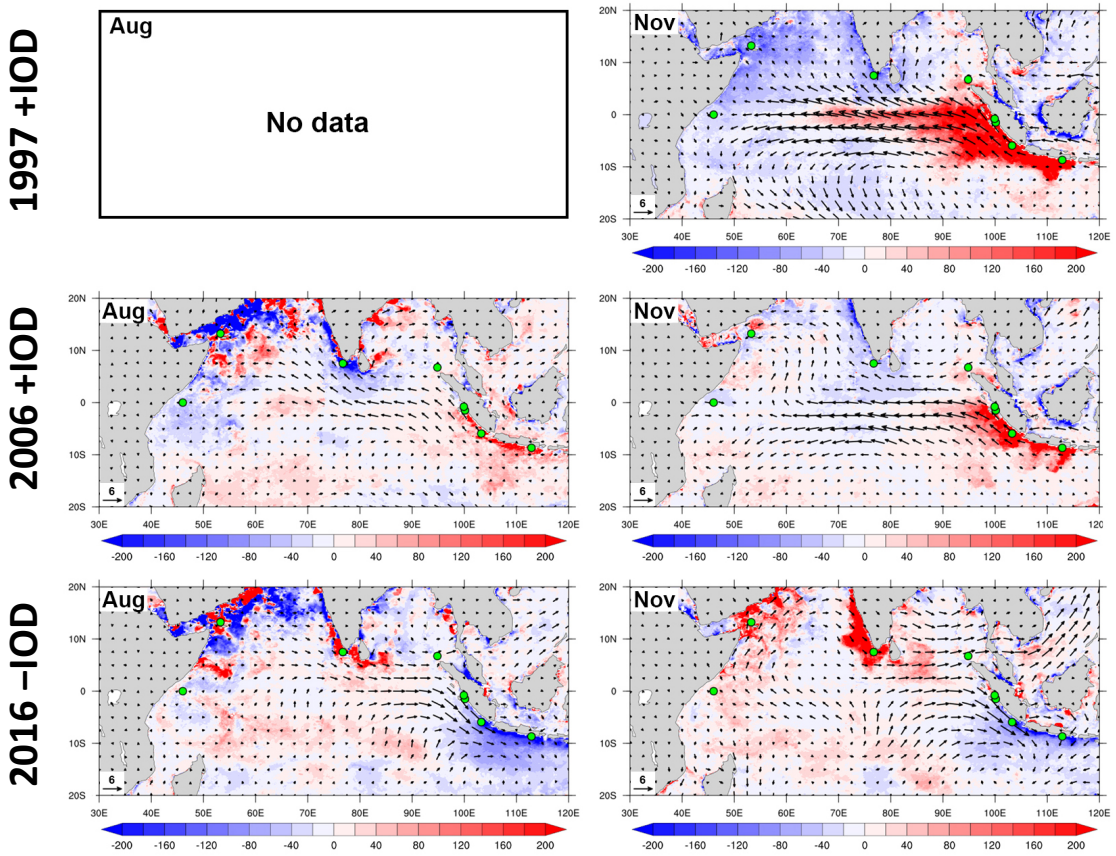
Upwelling intensity

Zonal wind intensity — **Zonal wind in the past**

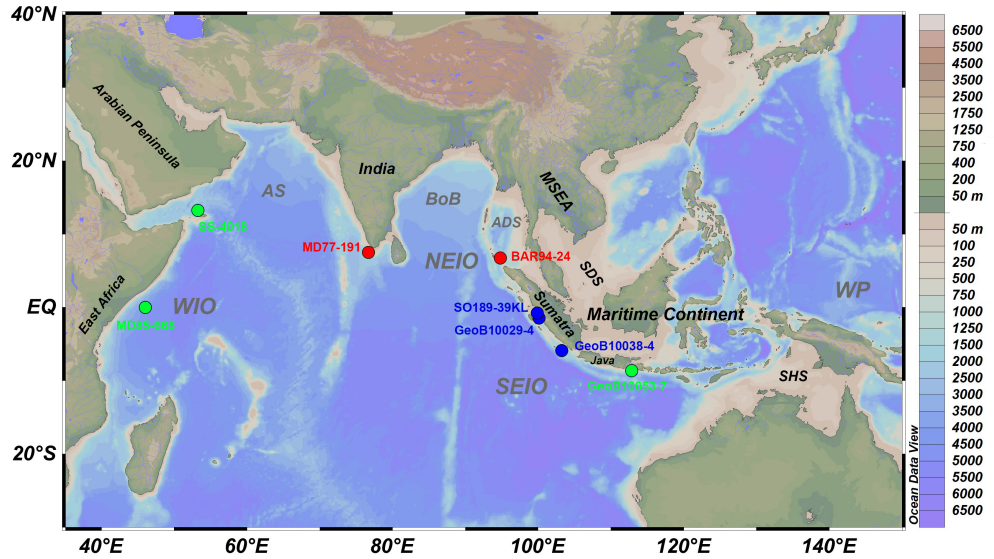
(a) Summer (MJJAS) and **(b)** winter (NDJFM) primary productivity (color, gC m^{-2} yr^{-1}) and SST (contours, °C)
Data: VGPM PP based on MODIS, 2003-2019 (Behrenfeld and Falkowski, 1997); NOAA OI SST V2, 2003-2019; ERA5, 2003-2019

Oceanic settings

Interannual anomaly



Monthly anomalies of primary productivity (color, gC m^{-2} yr^{-1}) and surface wind (vectors, m/s)
Data: VGPM PP based on MODIS, 2003-2019 (Behrenfeld and Falkowski, 1997); ERA5, 2003-2019



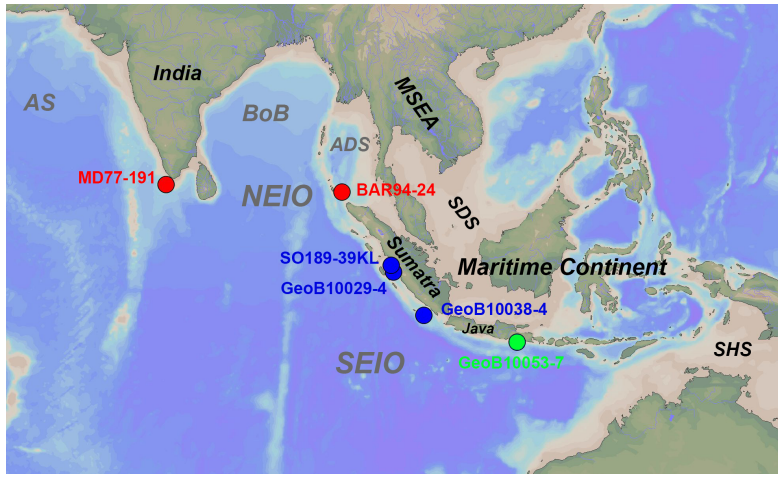
Positive IOD
↓
Easterly anomalies
↓
Higher PP (BAR94-24) **Lower PP (MD77-191)**

Negative IOD
↓
Westerly anomalies
↓
Lower PP (BAR94-24) **Higher PP (MD77-191)**

Oceanic settings

SW Sumatra: core GeoB10038-4

W (equatorial) Sumatra: cores SO189-39KL, GeoB10029-4



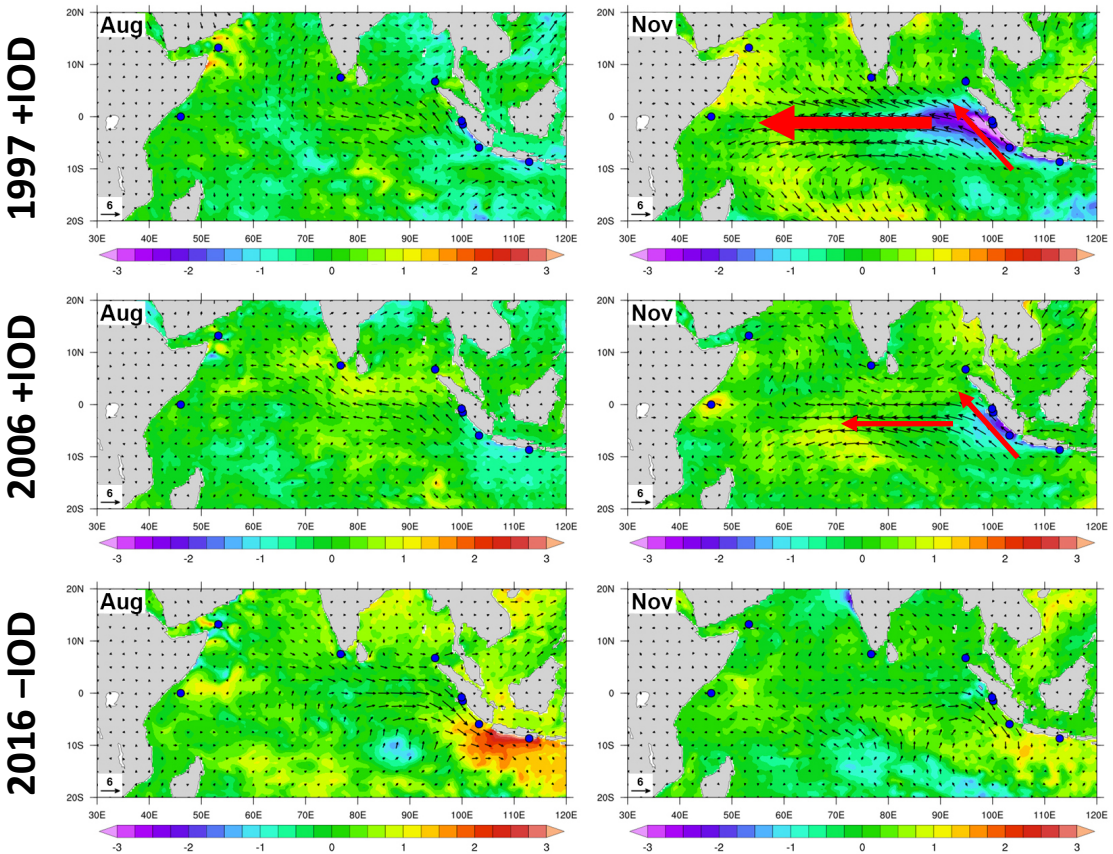
Positive vs Negative IOD

Alongshore vs Equatorial winds

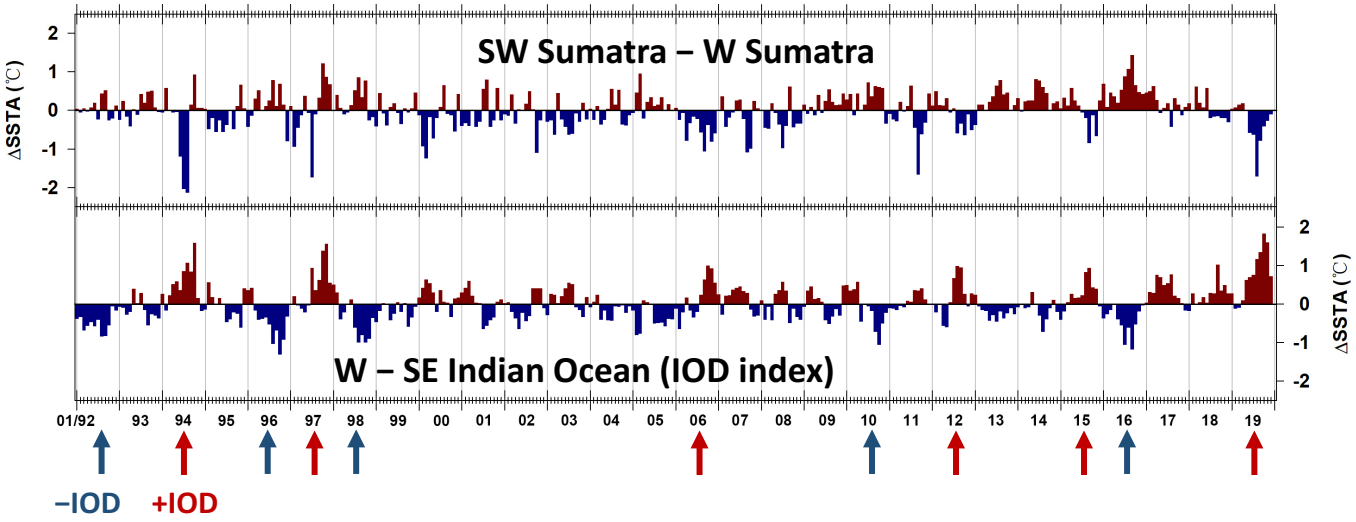
↓

SW – W Sumatra SSTA

Interannual anomaly



Differences of SST anomalies



Monthly anomalies of primary productivity (color, gC m^{-2} yr^{-1}) and surface wind (vectors, m/s)
Data: NOAA OI SST V2, 2003-2019; ERA5, 2003-2019

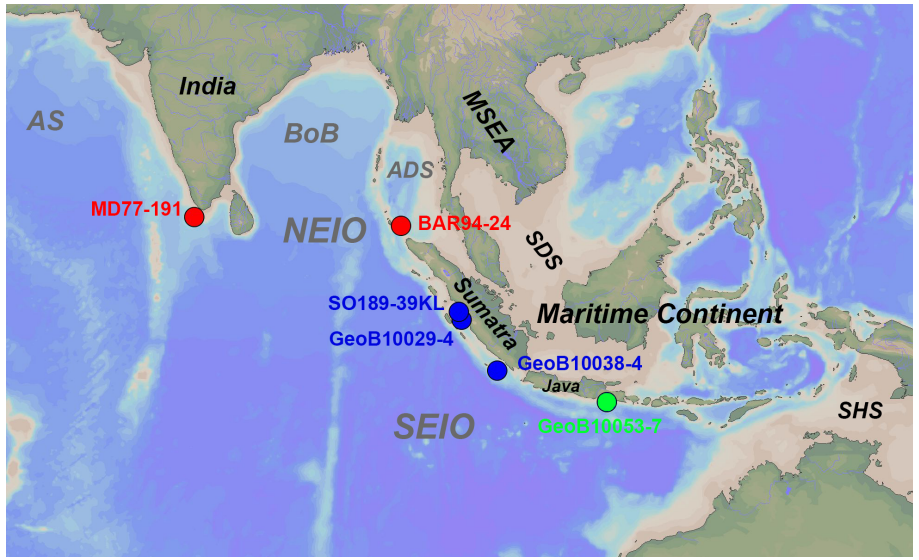
Positive IOD → Negative ΔSSTA → Stronger cooling off SW Sumatra

Negative IOD → Positive ΔSSTA → Stronger warming off SW Sumatra

→ Alongshore southeasterly (northwesterly) dominates

1997 +IOD → Positive ΔSSTA → Stronger cooling off W Sumatra → Equatorial easterly dominates

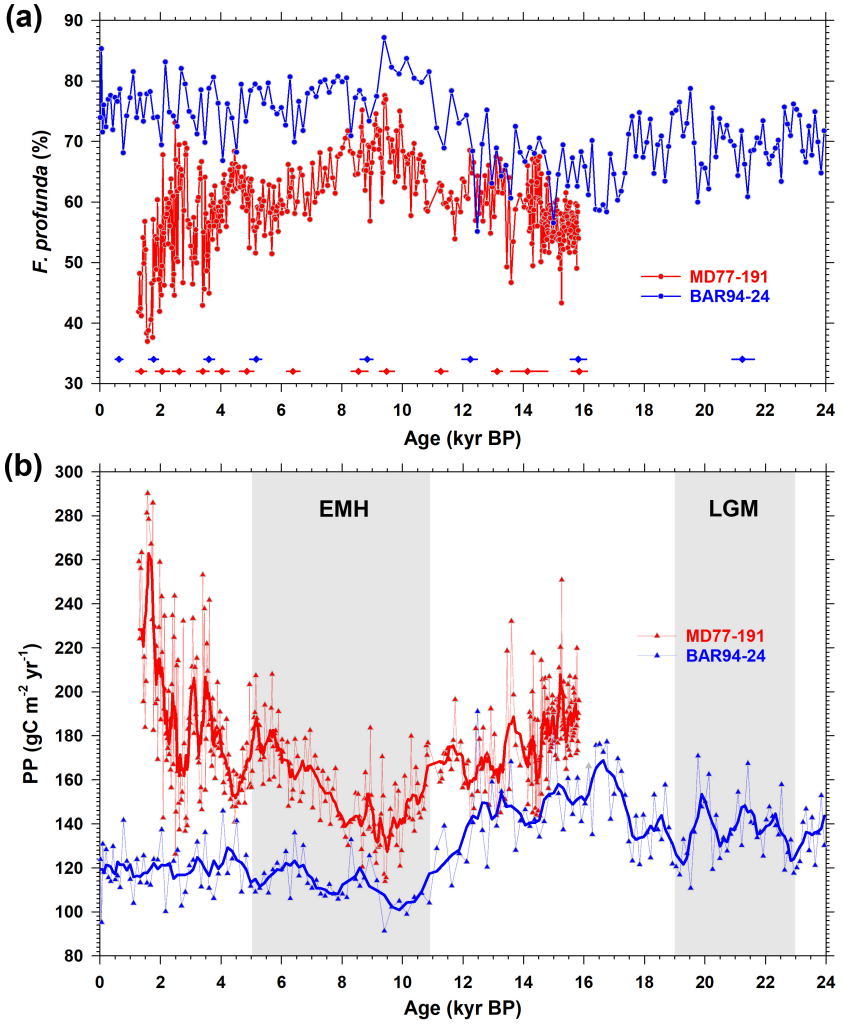
Reconstructed PP



MD77-191
An increasing trend over the Holocene

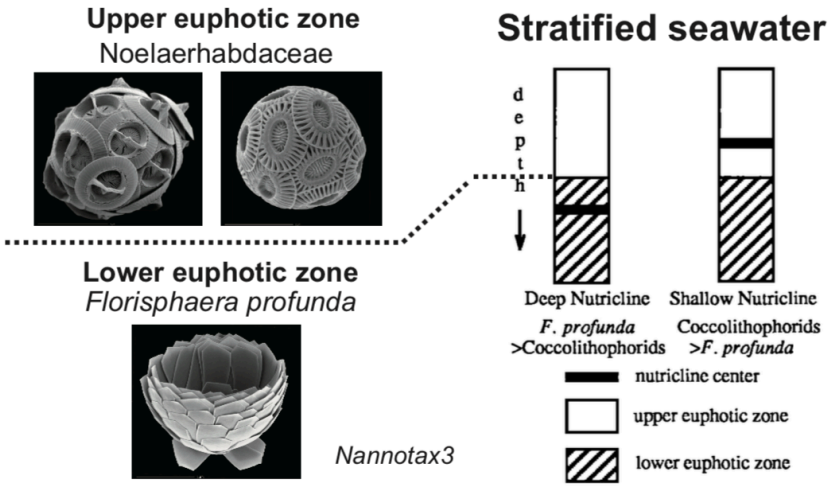
BAR94-24
LGM PP higher than Holocene

Cores MD77-191, BAR94-24 PP

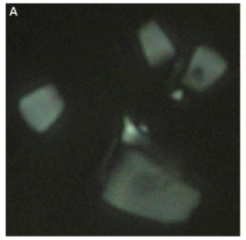


Fp%-PP empirical equation

Coccolithophores





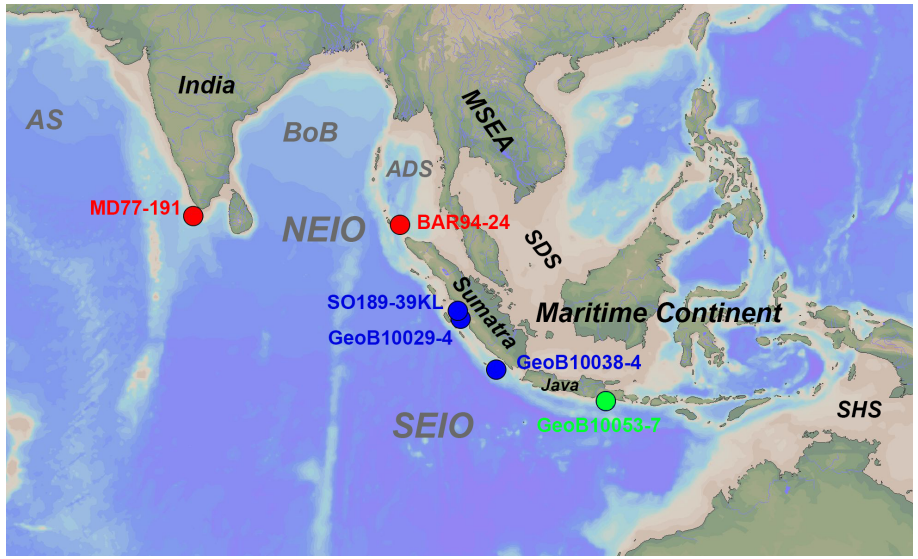


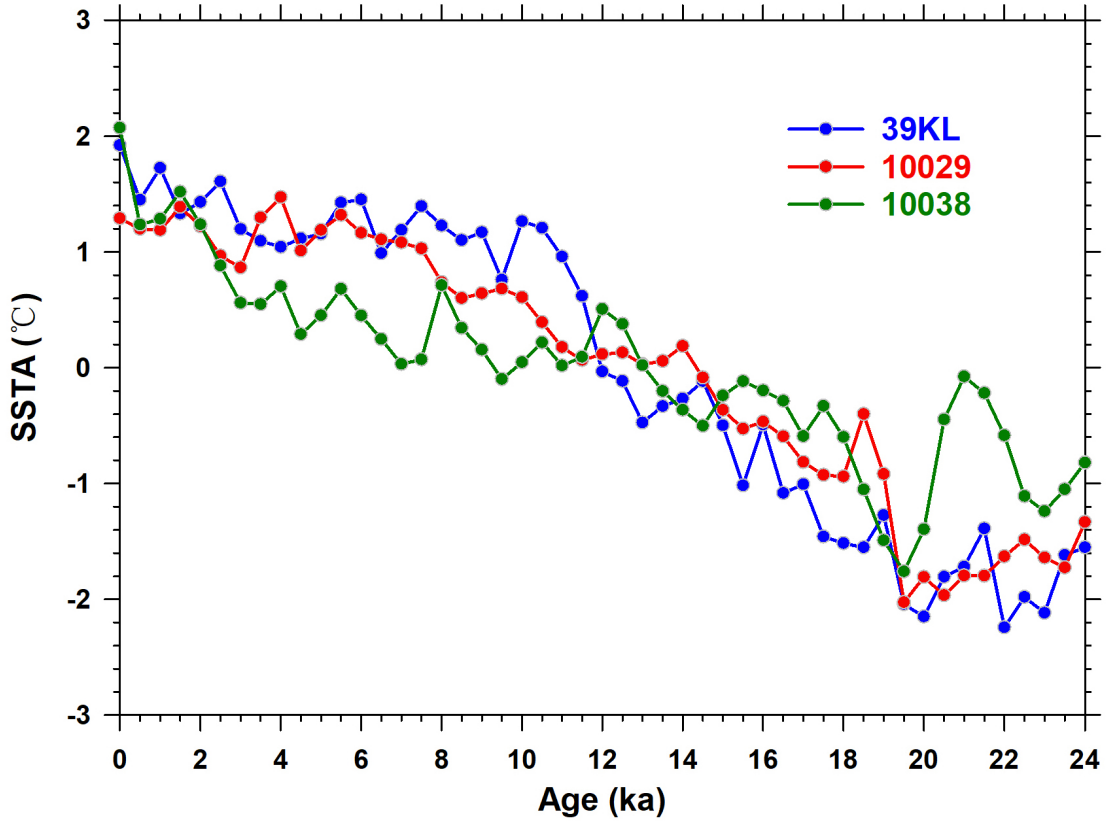
$$Fp\% = N_{Fp}/N_{total} \times 100$$

$$PP = 10^{[3.11-0.27\times(Fp\%)]}$$

Molfino et al., 1990;
Hernández-Almeida et al, 2019

Reconstructed SSTA





SST data are from Mohtadi et al., 2010, 2014, calculated by Mg/Ca of *G. ruber*.

$SSTA = SST - \overline{SST}_{0\text{-}24\ ka}$

Discussion

PP in the western Indian Ocean

LGM: lower sea level

BAR94-24 +PPA

↓

Stronger easterly

↓

Weaker Walker circulation ↔ **Equatorial easterly dominates**

+ΔSSTA

↓

1997 IOD-like mean state

Early-middle Holocene: smaller precession

MD77-191 −PPA

↓

Weaker westerly

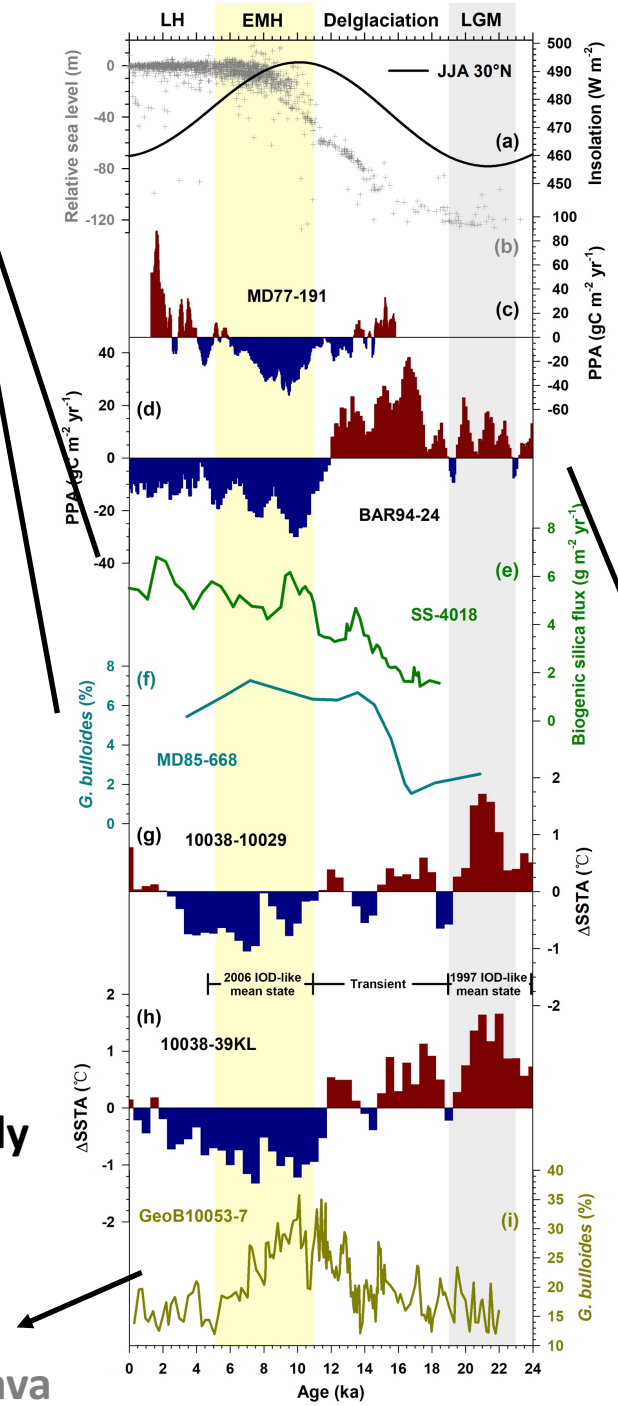
↓

Weaker Walker circulation ↔ **Alongshore southeasterly dominates**

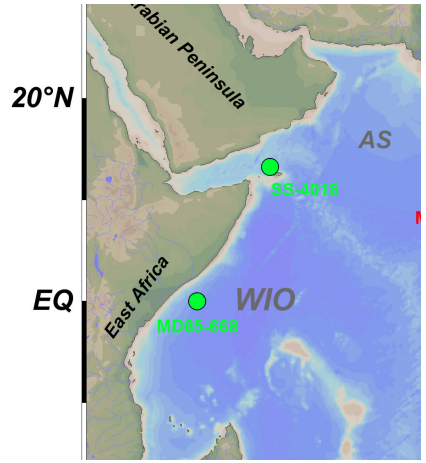
−ΔSSTA

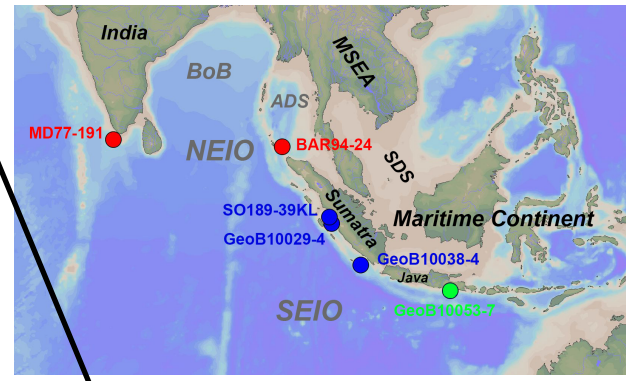
↓

2006 IOD-like mean state



Easterly off Java





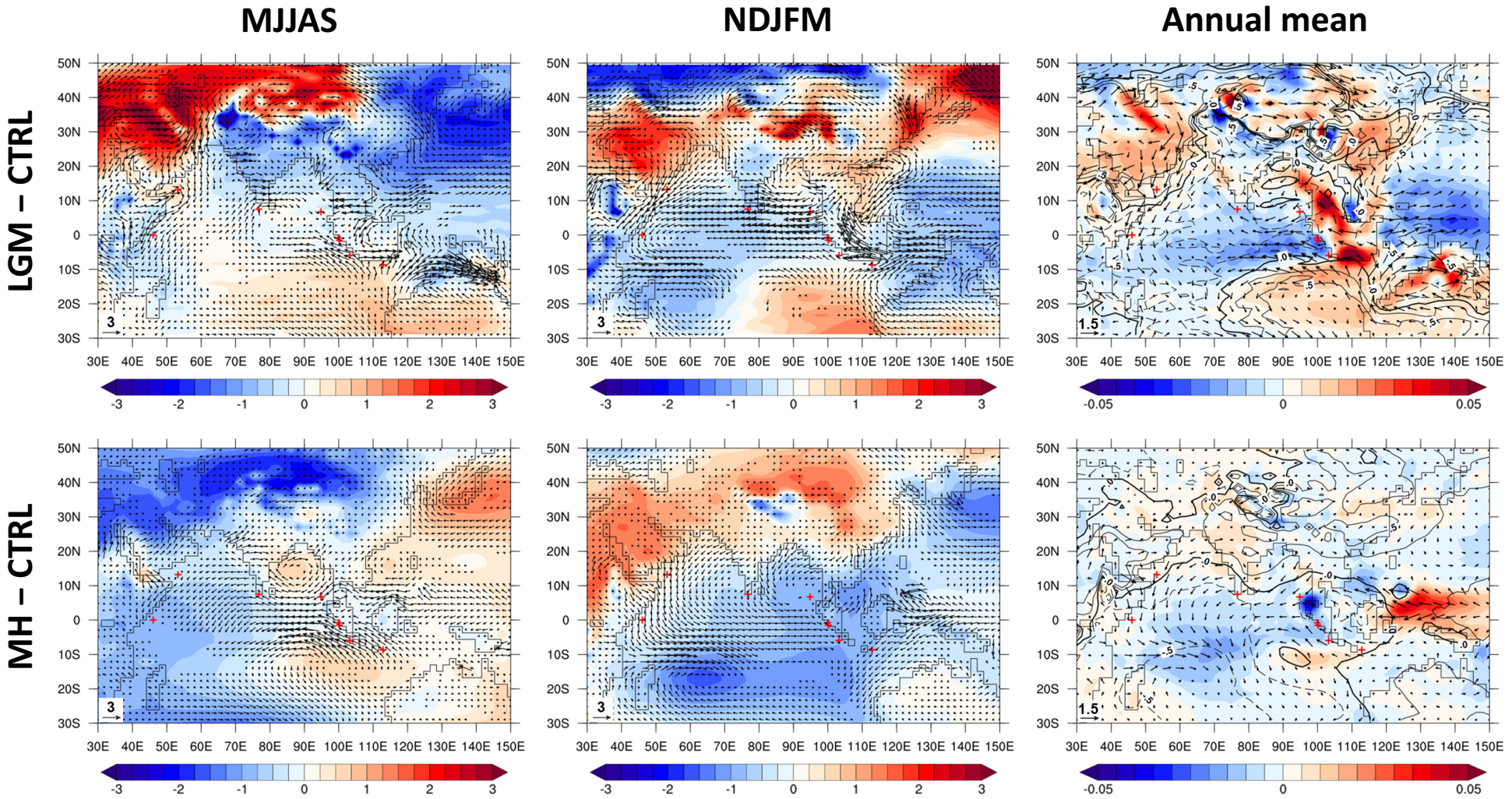
$$PPA = PP - \overline{PP}_{\text{whole interval}}$$

Hibbert et al., 2018
Balaji et al., 2018
Vergnaud Grazzini et al., 1995
Mohtadi et al., 2011

Discussion

Paleoclimate simulations run with earth system model AWI-ESM-1-1-LR (Lohmann et al., 2020; Shi et al., 2020)

Set-ups of Last Glacial Maximum (LGM), Mid-Holocene (MH), and pre-industrial period (CTRL)(Kageyama et al., 2017)



Equatorial easterly anomalies in winter & Alongshore southeasterly anomalies in summer

↓

Weaker Walker circulation

Equatorial easterly & Alongshore southeasterly anomalies in summer

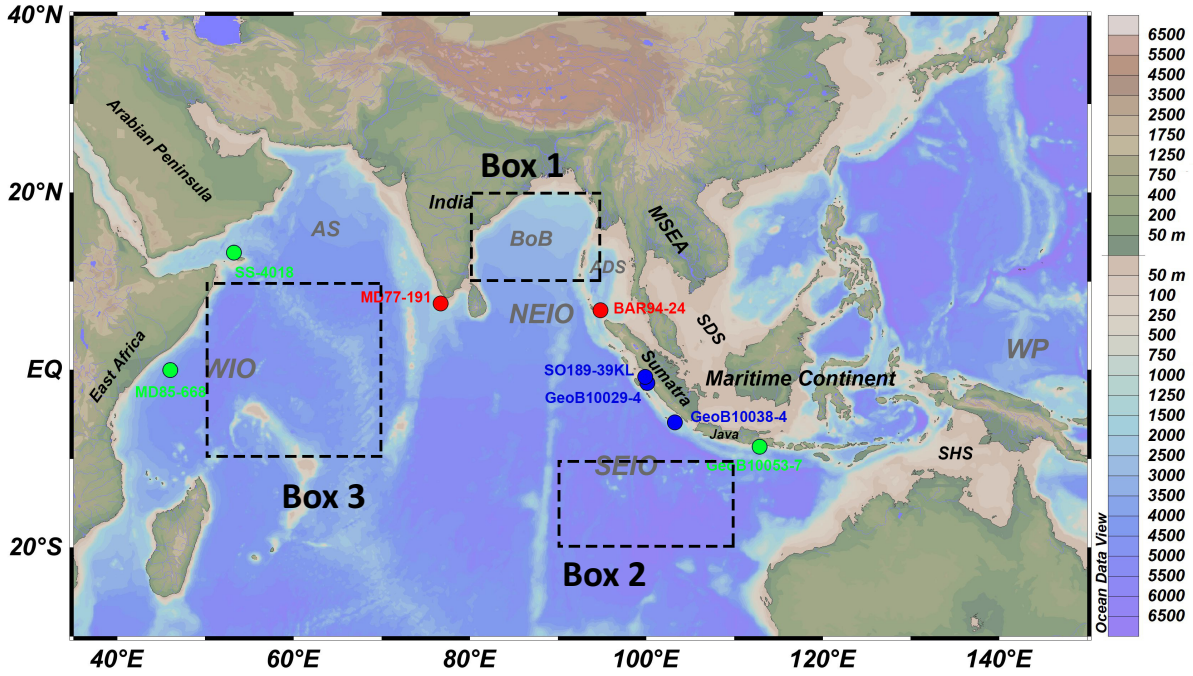
↓

Weaker Walker circulation

Sea level pressure (color, hPa), surface wind (vectors, m/s)

Vertical velocity at 500 hPa (color, Pa/s), surface wind (vectors, m/s), sea level pressure (contours, hPa)

Discussion



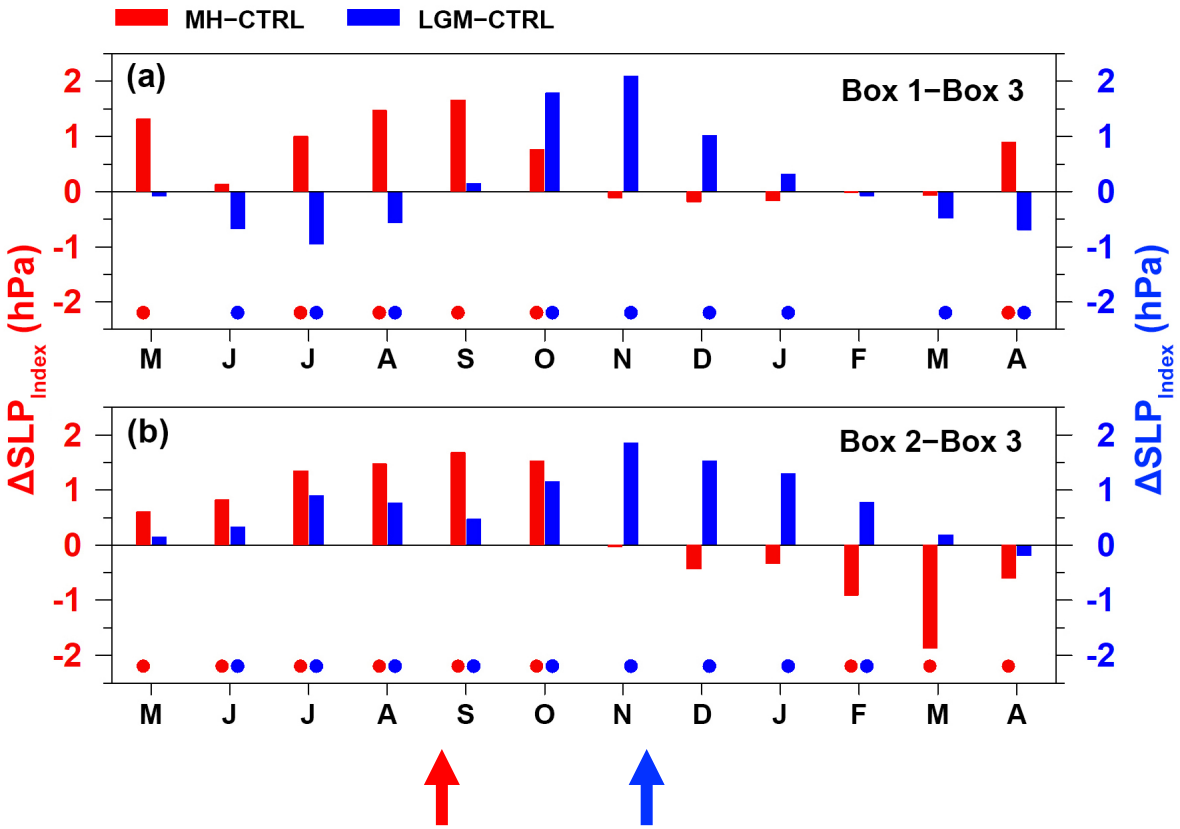
Zonal gradient over the tropical Indian Ocean

SLP indices Box 1–3, 2–3 ⟷ Indian Ocean Walker circulation

↓

ΔSLP indices Box 1–3, 2–3

Paleoclimate simulations run with AWI-ESM-1-1-LR



Effect of smaller precession

Effect of lower sea level

Different boundary conditions

Conclusions

1. Indian Ocean Walker circulation during the LGM and Early-middle Holocene was weaker than present.

2. During the LGM, the weaker Walker circulation appears to be dominated by strong anomalous equatorial easterlies in early winter, in a similar way as the positive IOD mean state observed in 1997.

3. During the EMH, anomalous equatorial easterlies and strong anomalous southeasterlies off Sumatra are detected in late summer, which appears to be similar to the positive IOD mean state of 2006.

4. The deglaciation might be a transient period in-between LGM and EMH.

References

Behrenfeld, M. J., Falkowski, P. G., 1997. Limnology and Oceanography 42, 1–20.
Hernández-Almeida, I., Ausín, B., Saavedra-Pellitero, M., Baumann, K.-H., Stoll, H. M., 2019. Quaternary Science Reviews, 205, 166–181.
Mohtadi, M., Steinke, S., Lückge, A., Groeneveld, J., Hathorne, E. D., 2010. Earth and Planetary Science Letters 292, 89−97.
Mohtadi, M., Oppo, D. W., Steinke, S., Stuut, J.-B. W., De Pol-Holz, R., Hebbeln, D., Lückge, A., 2011. Nature Geoscience 4, 540−544.
Mohtadi, M., Prange, M., Oppo, D. W., De Pol-Holz, R., Merkel, U., Zhang, X., Steinke, S., Lückge, A., 2014. Nature 509, 76−80.
Molfino, B., McIntyre, A., 1990. Science 249, 766–769.
Hibbert, F., Williams, F., Fallon, S., Rohling, E. J., 2018. Scientific Data 5, 180088.
Balaji, D., Bhushan, R., Chamyal, L. S., 2018. Climate of the Past 14, 1331−1343.
Vergnaud Grazzini, C. V., Vénec-Peyré, M. T., Caulet, J. P., Lerasle, N., 1995. Marine Micropaleontology 26, 137−152.
Lohmann, G., Butzin, M., Eissner, N., Shi, X., Stepanek, C., 2020. Paleoceanography and Paleoclimatology 35, e2019PA003782.
Shi X., Lohmann G, Sidorenko D, Yang H.,2020. The Holocene 30, 996–1015.
Kageyama, M., et al., 2017. Geoscientific Model Development 10, 4035–4055.